Analyst

ROYAL SOCIETY OF CHEMISTRY

PAPER

View Article Online
View Journal | View Issue

Cite this: *Analyst*, 2024, **149**, 3793

Mobility capillary electrophoresis–native mass spectrometry reveals the dynamic conformational equilibrium of calmodulin and its complexes†

Yi Zhao,[a] Wenjing Zhang, [a] Jie Hong,[b] Lei Yang, [a] Yuanyuan Wang,[c] Feng Qu*[d] and Wei Xu *[a]

Received 10th March 2024,
Accepted 19th May 2024

DOI: 10.1039/d4an00378k

rsc.li/analyst

Benefitting from the rapid evolution of artificial intelligence and structural biology, an expanding collection of high-resolution protein structures has greatly improved our understanding of protein functions. Yet, proteins are inherently flexible, and these static structures can only offer limited snapshots of their true dynamic nature. The conformational and functional changes of calmodulin (CaM) induced by Ca^{2+} binding have always been a focus of research. In this study, the conformational dynamics of CaM and its complexes were investigated using a mobility capillary electrophoresis (MCE) and native mass spectrometry (native MS) based method. By analyzing the ellipsoidal geometries of CaM in the solution phase at different Ca^{2+} concentrations, it is interesting to discover that CaM molecules, whether bound to Ca^{2+} or not, possess both closed and open conformations. Moreover, each individual CaM molecule actively "jumps" (equilibrium exchange) between these two distinct conformations on a timescale ranging from milli- to micro-seconds. The binding of Ca^{2+} ions did not affect the structural dynamics of CaM, while the binding of a peptide ligand would stabilize CaM, leading to the observation of a single, compact conformation of the resulting protein complex. A target recognition mechanism was also proposed based on these new findings, suggesting that CaM's interaction with targets may favor a conformational selection model. This enriches our understanding of the binding principles between CaM and its numerous targets.

Introduction

CaM interacts and modulates the function of hundreds of effector proteins in a Ca^{2+}-dependent manner. This unique ability allows CaM to act as a Ca^{2+} sensor, modulating the activity of various proteins involved in processes such as neurotransmitter release, muscle contraction, cell differentiation, apoptosis, and gene transcription.[1–6] It is well known that CaM has two globular domains connected by a flexible linker. Each domain comprises a pair of EF hand motifs that could bind with two Ca^{2+}.[7–10] CaM is conventionally believed to adopt different conformations upon binding with Ca^{2+}, which then enables further interaction with target proteins. Extensive research studies have been conducted to investigate the relationship between the structure and function of CaM, and a multitude of CaM structures and their associated complexes have been documented in the Protein Data Bank (PDB). Based on these results, it is generally believed that both Ca^{2+}-free and Ca^{2+}-bound CaM have open conformations, where the N- and C-terminal lobes of CaM are separated by a central linker[8,11–13]; besides forming hydrophobic pockets within each lobe, the binding of $4Ca^{2+}$ would reorganize the intrinsically disordered central linker into an alpha helix[14–16]; this central linker transitions back to an intrinsically disordered region (IDR) upon binding to targets;[3,17,18] both open and closed conformations have been observed for CaM within complexes, and all the closed conformations are associated with the addition of $4Ca^{2+}$.[19–23]

Nonetheless, the structure of proteins is not static and can exhibit variability across multiple levels, encompassing local fluctuations to significant conformational changes,[24,25] particularly in the case of intrinsically disordered proteins (IDPs) or proteins featuring IDRs. Ca^{2+} binding and target recognition depend heavily on the structural dynamics of CaM. Techniques, including time-resolved small-angle X-ray scattering,[4,26,27] nuclear magnetic resonance (NMR) relaxation

---

[a] School of Medical Technology, Beijing Institute of Technology, Beijing 100081, China. E-mail: weixu@bit.edu.cn
[b] Kunshan Nier Precision Instrumentation Inc. Kunshan, Suzhou, 215316, China
[c] College of Traditional Chinese Medicine, Shandong University of Traditional Chinese Medicine, Jinan, 250355, China
[d] School of Life Science, Beijing Institute of Technology, Beijing 100081, China. E-mail: qufengqu@bit.edu.cn

† Electronic supplementary information (ESI) available. See DOI: **https://doi.org/10.1039/d4an00378k**

methods,[28–30] single molecule fluorescence resonance energy transfer (FRET)[31,32] and cross-linking mass spectrometry,[33,34] have been applied to explore the structural dynamics of CaM. The intermediate conformational state and a wide range of interdomain distances were sampled. However, these techniques can only provide static structures of CaM. Therefore, this has led to the proposal that the binding of either Ca^{2+} or a ligand may shift a pre-existing structural equilibrium of CaM, instead of following a stepwise structure evolution.[25] However, the precise characteristics of protein structural dynamics, including those of CaM, continue to be a complex and actively researched subject, sparking ongoing debates and discussions.

Many new methods have been used to study the dynamics of proteins.[35–39] Native MS enables deep understanding of their structures, interactions, and conformational dynamics.[40–49] More recently, MCE has been developed and coupled together with native MS to study the ellipsoid geometric structures of proteins, as well as protein structure evolutions in different solvent environments.[50–54] In this study, the conformational dynamics of apo-CaM and Ca^{2+}-bound CaM, as well as their binding events with a peptide ligand were investigated. Both MCE and native MS experiments were carried out for CaM samples at different Ca^{2+} concentrations. The formation of $n$$Ca^{2+}$–CaM as well as their ellipsoid geometries were characterized. Furthermore, we examined the influence of pH and temperature on these complexes. Finally, stoichiometric and conformational analyses were carried out for mixtures of CaM and the peptide ligand in the presence of Ca^{2+} at various concentrations, offering valuable insights for further research into the mechanisms of CaM–ligand interactions.

Results and discussion

Conformational dynamics of apo-CaM

X-ray and NMR studies have found that the crystal structures of CaM (such as 1CFD, 1CFC, 1DMO) have an open conformation where the N- and C-terminal lobes are separated by a flexible linker.[8,11] To explore the structural dynamics of apo-CaM, MCE and native MS experiments were then carried out. MCE separates ions based on their hydrodynamic radii and effective charges in solvent,[51] and although protein structures may change during the transition from a liquid to a gas phase, the charge-state distributions (CSDs) in native MS experiments still provide valuable protein structure information, specifically solvent-accessible surface areas (SASAs), which can be deduced from the mass spectra.[55–57] Typically, globular proteins exhibit charge-state distributions with a single charge group, while IDPs have charge-state distributions with more charge groups.[58–60] As shown in Fig. 1a, the two peaks in the MCE electropherogram correspond to the neutral marker (phenol) and apo-CaM, respectively. According to MCE results, apo-CaM may only have one conformation, which is consistent with X-ray findings. However, three charge groups, labelled as charge group 1, 2 and 3, were observed for apo-CaM in its native mass spectrum (Fig. 1b), and their average charge states (Z_{av}) were 7.53, 11.67 and 18.31, respectively (Fig. S1†). Native MS results suggest that apo-CaM has multiple conformations: either three conformations that all behave like globular proteins, or two conformations of which one behaves like a globular protein with a single charge group and the other behaves like an IDP exhibiting two charge groups. Additional size exclusion chromatography (SEC) experiments were also carried out,

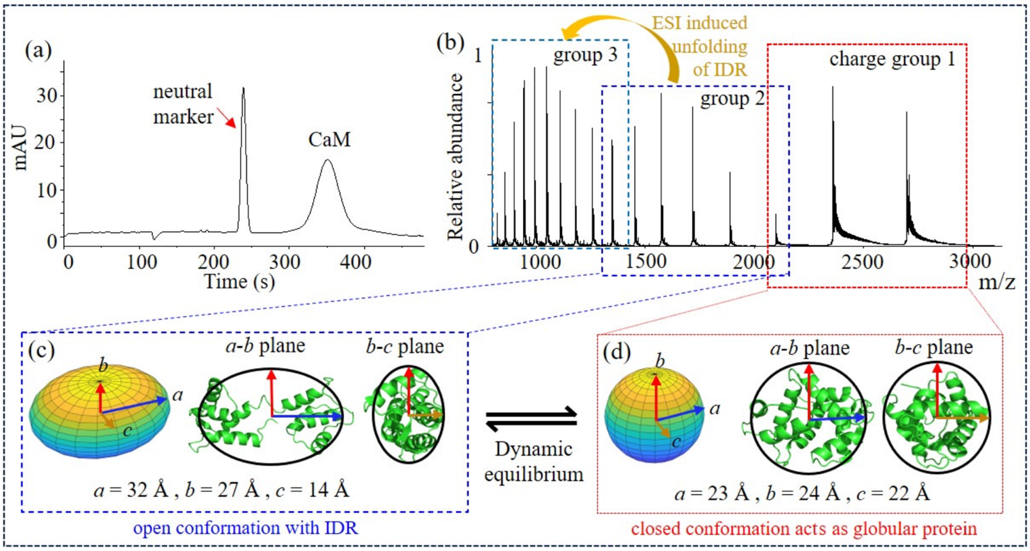

Fig. 1 Conformational dynamics of apo-CaM. (a) MCE of apo-CaM, 30 mbar and 15 kV; (b) native mass spectrum of apo-CaM; (c) and (d) ellipsoids of the open and closed conformations corresponding to charge groups 2 and 1, respectively. Ellipsoids are fitted and compared with PDB structures 1CFD[8] and 1PRW.[61]

and a single chromatography peak was observed for apo-CaM (Fig. S2†), which is in agreement with the MCE result but not the native MS result.

To elucidate the conflicting experimental results of a single peak in MCE and size exclusion chromatography experiments with a multi charged-state distribution in native MS, based on previous research and our subsequent analysis of experimental results, we propose that apo-CaM possesses two conformations under dynamic equilibrium (Fig. 1c and d): charge group 1 corresponds to a closed conformation that behaves like a globular protein; charge group 2 corresponds to an open conformation that has IDRs, and group 3 results from further unfolding of CaM with IDRs (group 2) during the ESI process. Furthermore, every single apo-CaM molecule would actively "jump" (dynamic equilibrium) between open and closed conformations in the solvent. Several lines of evidence support this hypothesis. First, both single-molecule fluorescence resonance energy transfer[62,63] and cross-linking MS[33,34] experiments found that a wide range of distances are sampled between the N- and C-terminals of CaM, indicating that CaM possesses multiple conformations in solution. By combining double electron–electron resonance electron paramagnetic resonance and molecular dynamic (MD) simulations, it has also been demonstrated that $4Ca^{2+}$–CaM could adopt multiple conformational substates.[64] Second, according to NMR studies, the linking region of CaM is flexible before binding to a ligand[11] and molecular dynamics simulations demonstrated that this CaM structure with a flexible linking region could further unfold during the ESI process and resulted in dual charge-state distributions in the mass spectrum.[65] Our subsequent findings also indicate that groups 2 and 3 exhibit similar traits in solution, which distinguish them from group 1 when adapting to dynamic environmental changes. Moreover, the ellipsoids calculated for charge groups 1 and 2 agree well with a closed and an open structure of CaM in the PDB, respectively (Fig. 1c and d, details could be found in Table S1†). The SASA calculated from charge-state distributions of group 3 (23 735.57 Å^2) is significantly higher than that of any crystal structure in the PDB, while groups 1 (6729.89 Å^2) and 2 (12 523.62 Å^2) show good correspondence with the SASA in the PDB. These data explain the origin of the three charge groups: charge groups 1 and 2 correspond to a closed and an open conformation of apo-CaM in solvent, respectively, while group 3 corresponds to the further unfolding of CaM during the ESI process (Fig. S3†). Next, if apo-CaM has two conformational states, why these two conformations are not separatable (Fig. 1a and S2†)? This could be due to the fact that the transition time for CaM molecules ranges from microseconds to milliseconds.[66–69] Within the same transition cycle, all CaM molecules have the same migration distance. Therefore, separation techniques that operate on a timescale of seconds, such as MCE and size exclusion chromatography, cannot differentiate between different conformations of CaM. As a result, different conformational states could be captured/sampled at specific time points using relatively fast techniques, such as fluorescence resonance energy transfer, cross-linking MS and native MS, but they could not be separated in MCE or size exclusion chromatography. Str2str[70] results further support our conclusion that, regardless of whether the input is 1PRW (Ca^{2+}-free) or 1CFD, Apo-CaM is always capable of interconverting between a closed conformation and an open conformation (Fig. S4†).

Conformational dynamics of Ca^{2+}-bound CaM

As an important Ca^{2+} signaling process, the binding of Ca^{2+} could induce structure reorganization within CaM, that might enable the following target recognition. With the identification of a closed conformation for $2Ca^{2+}$–CaM and open conformations for $4Ca^{2+}$–CaM (such as 3CLN, 1CLL), it has been suspected that the binding events of Ca^{2+} may induce step-wise structure evolution[71] or shift the pre-existing structure equilibrium:[25] from an open structure (apo-CaM) to a closed structure ($2Ca^{2+}$–CaM) and back to open structure states ($4Ca^{2+}$–CaM). To investigate the conformational dynamics of $n\mathrm{Ca}^{2+}$–CaM, MCE and native MS experiments were conducted on CaM samples that had been incubated with varying concentrations of Ca^{2+}. First, similar MCE results were acquired, in which single protein chromatography peaks were observed (Fig. 2a). As shown in Fig. 2b, CaM will bind to more Ca^{2+} with increased Ca^{2+} concentrations. apo-CaM, $2Ca^{2+}$–CaM, and $4Ca^{2+}$–CaM were found to be dominant peaks when the concentration ratios of CaM : Ca^{2+} were 1 : 1, 1 : 1.5 and 1 : 3, respectively. More data for other concentration ratios were plotted, as shown in Fig. S5.† As shown in Fig. 2b, $n\mathrm{Ca}^{2+}$–CaM complexes with varying numbers of Ca^{2+} (n ranging from 0 to 4) consistently exhibit three charged groups in their native mass spectra, indicating that $n\mathrm{Ca}^{2+}$–CaM complexes have similar conformational dynamics to that of apo-CaM. Therefore, similar to apo-CaM, $n\mathrm{Ca}^{2+}$–CaM all have two dynamically exchanged conformational states: open and closed conformations. The closed conformations act like globular proteins, while the open conformations have IDRs. After applying multi-Gaussian fitting to the MCE electropherogram, the ellipsoid geometries of the closed and open conformations of $n\mathrm{Ca}^{2+}$-CaM complexes are plotted and compared in Fig. 2c and 2d, respectively. Statistically significant differences in the a, b, and c axes of the ellipsoid geometries of the closed and open conformations of $n\mathrm{Ca}^{2+}$–CaM were analyzed using GraphPad Prism 8. It was interesting to find that ellipsoid geometries of $2Ca^{2+}$–CaM and $4Ca^{2+}$–CaM have no statistical difference with those of apo-CaM (p values: 0.10, 0.81 and 0.98 for a, b and c in Fig. 2c; 0.07, 0.54 and 0.58 for a, b and c in Fig. 2d). As there was no apparent decrease in ion intensities for charge group 3, it raised suspicion that the proportion of IDRs remained unchanged after binding with Ca^{2+}. In conclusion, the binding events of Ca^{2+} with CaM do not significantly change the conformational dynamics of CaM or $n\mathrm{Ca}^{2+}$–CaM complexes.

Besides increasing Ca^{2+} concentration, the conformational dynamics of $n\mathrm{Ca}^{2+}$–CaM in different solvent environments, including varying pH and temperature, were further explored. The relative proportions of $n\mathrm{Ca}^{2+}$–CaM complexes within the three charge groups under different solvent conditions are illustrated in Fig. 3 (please refer to Fig. S6–7 and Tables S2–

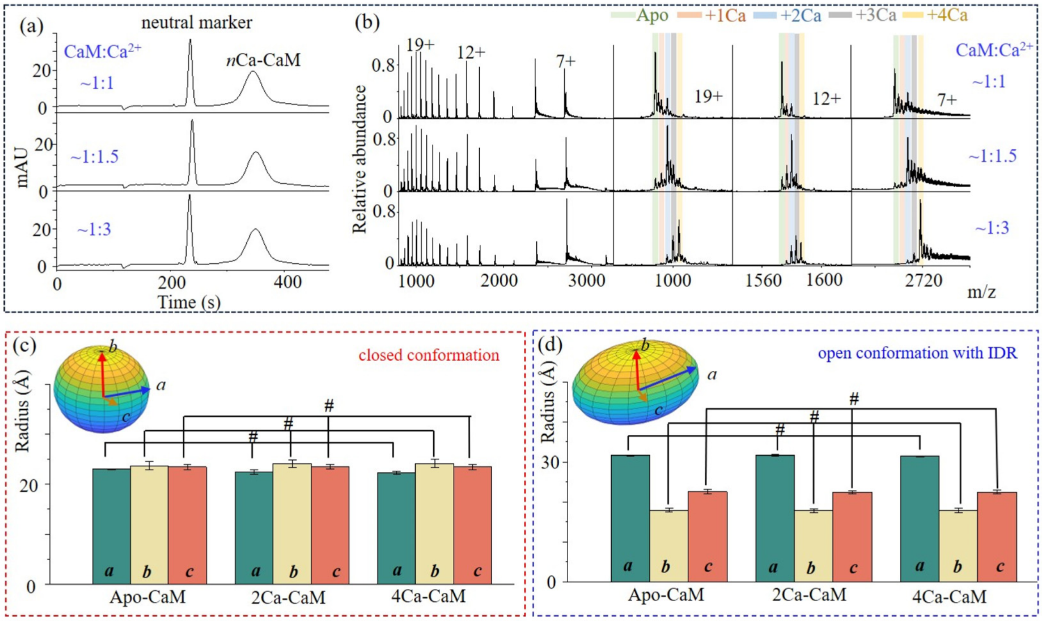

#: no statistical difference, $p > 0.05$

Fig. 2 Conformational dynamics of $n\text{Ca}^{2+}$–CaM complexes. (a) and (b) MCE and native MS results of CaM samples with different CaM : Ca^{2+} ratios: 1 : 1, 1 : 1.5 and 1 : 3; (c) and (d) ellipsoid radii (*a*, *b*, and *c*) of the closed and open conformations of $n\text{Ca}^{2+}$–CaM complexes.

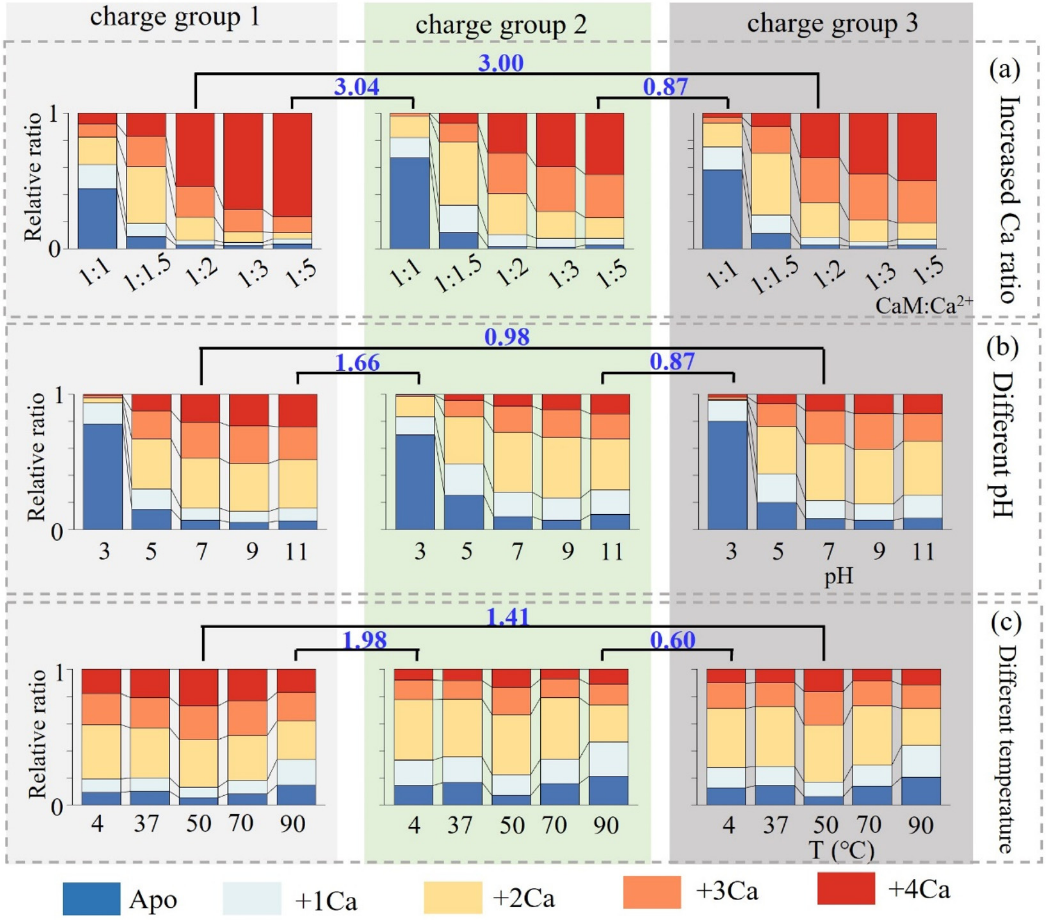

Fig. 3 Relative proportions of $n\text{Ca}^{2+}$–CaM under different solvent conditions and the Manhattan distances between different charge groups: (a) with increased Ca^{2+} ratio; (b) at different pH; and (c) at different temperatures.

S10† for detailed information). Since different charge groups correspond to different CaM conformations, the similarity of the Ca^{2+}-binding abilities of the three groups was first characterized using the Manhattan distance method. In all cases, groups 2 and 3 have a smaller Manhattan distance than that between groups 1 and 2 or 1 and 3, confirming that groups 2 and 3 originate from one group of ions with similar conformations in solvents. As depicted in Fig. 2b and 3, CaM possessing the closed conformation (group 1) also exhibits different binding preferences with Ca^{2+}, preferring to bind 2 and 4 Ca^{2+}. In comparison, CaM having the open conformation (groups 2 and 3) shows no such preferences, and a gradual increase of Ca^{2+} binding numbers was observed by increasing Ca^{2+} concentrations. Fig. S8† presents the K_d fitting curves for different charge states, and the corresponding K_d values are listed in Table S11.† These values were of the same order of magnitude as those reported in the references.[72,73] Furthermore, it is observed that group 1 does exhibit a notably stronger affinity towards Ca^{2+}, indicating that $4Ca^{2+}$–CaM is more inclined to adopt a closed conformation.[74] As depicted in Fig. S6,† the binding of Ca^{2+} to CaM hindered at lower pH, especially at 3.0, because its isoelectric point is approximately 4.0, resulting in a positively charged state for CaM at this acidic pH level. On the other hand, elevated temperatures, such as 50 °C, enhance the binding ability to Ca^{2+}, leading to an increase in the relative ratio of $4Ca^{2+}$–CaM from 8% to 11%. However, excessively high temperatures (~90 °C) may lead to protein denaturation. It is worth noting that alterations in Ca^{2+} concentration, temperature and pH did not appear to significantly affect the conformational distribution of CaM (Fig. S9†).

CaM binding with a ligand

The structural flexibility of CaM is believed to account for its ability to recognize various targets, and the concentration of Ca^{2+} is also critical during this process.[75–78] The binding event of CaM with a peptide ligand, Mel, was then explored. The MCE and native MS results of CaM–Mel mixtures (1 : 1) at different Ca^{2+} concentrations are plotted in Fig. 4a and b. At a relatively low Ca^{2+} concentration (CaM : Ca^{2+} = 1 : 1), a fraction of CaM binds with Mel, and both $3Ca^{2+}$–CaM–Mel and $4Ca^{2+}$–CaM–Mel complexes are observed in the mass spectrum. As the Ca^{2+} concentration increases, a larger proportion of CaM associates with Mel, and the relative intensities of $3Ca^{2+}$–CaM–Mel decrease or even become unobservable when the Ca^{2+} concentration is high enough (CaM : Ca^{2+} = 1 : 3, Fig. 4d). As shown in Fig. 4a, $n$$Ca^{2+}$–CaM and $n$$Ca^{2+}$–CaM–Mel were separated in MCE, suggesting that Mel could stabilize the structure of CaM. Fig. 4c illustrates the ellipsoid shape of $4Ca^{2+}$–CaM–Mel, which was also compared with its crystal structure in the PDB (8AHS).[79] Instead of "jumping" between two conformations, CaM–Mel complexes adopt a relatively stable, closed conformation.

Based on the presented results, we proposed a target recognition mechanism for the interaction of CaM with Mel. As illustrated in Fig. 5, this mechanism aligns closely with the conformational selection model.[80,81] However, it has been traditionally believed that Ca^{2+} binding induces conformational changes in CaM, facilitating its interaction with target mole-

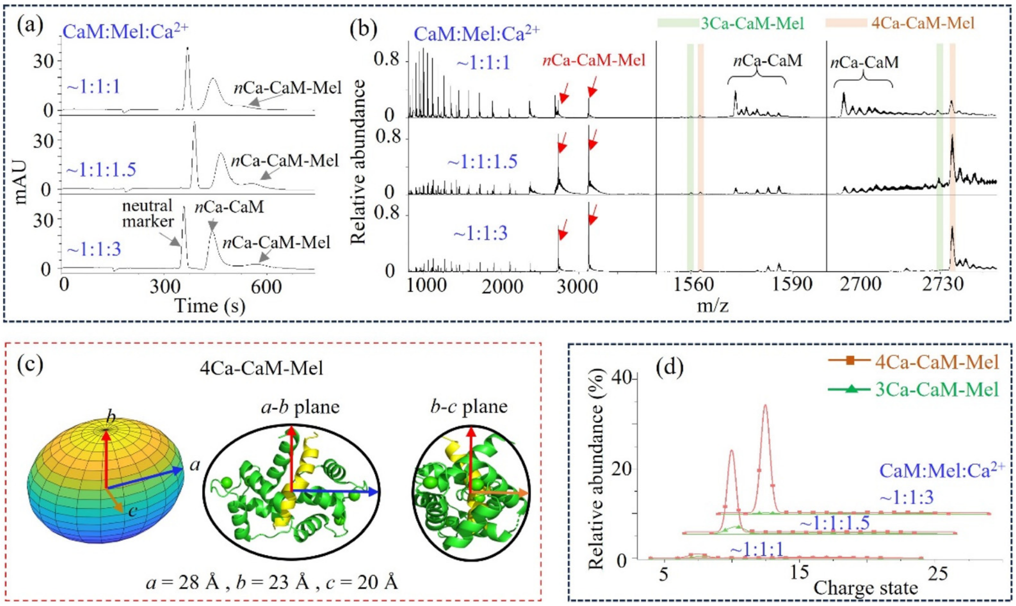

Fig. 4 CaM binding with a ligand, Mel. (a) and (b) MCE and native MS results of CaM–Mel mixtures at different Ca^{2+} concentrations; (c) ellipsoid shape and radii of $4Ca^{2+}$–CaM–Mel, as well as its comparison with its crystal structure in the PDB (8AHS, Table S1†); and (d) relative abundance of $3Ca^{2+}$–CaM–Mel and $4Ca^{2+}$–CaM–Mel complexes at different Ca^{2+} concentrations.

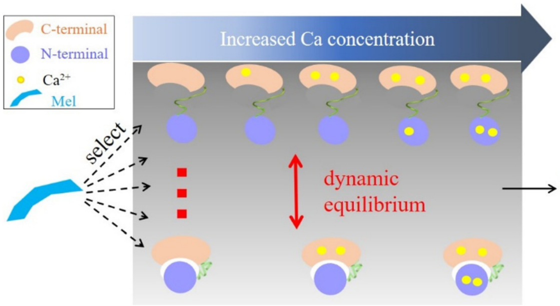

Fig. 5 Schematic illustration of the target recognition mechanism of CaM with Mel.

cules. Our results show that the binding of Ca^{2+} does not markedly alter the conformational dynamics of CaM. Both apo-CaM and $n$$Ca^{2+}$–CaM transition between different conformations. As a result, a target molecule may select and align with its preferred $n$$Ca^{2+}$–CaM conformation. This binding event then shifts the dynamic conformational equilibrium of CaM, which explains the wide range of targets that CaM could recognize. Furthermore, the presence and concentration of Ca^{2+} also play important roles in terms of providing hydrophobic pockets in the C- and N-terminal lobes.[82–85] These pockets can engage with an array of hydrophobic groups present on target molecules, promoting complex formation. This proposed mechanism was also supported by the fact that different CaM complexes harbor varying numbers of Ca^{2+}.[3,17,18,22,86–89] Notably, some ligands, such as the IQ motif of the human cardiac sodium channel $Na_v1.5$, even demonstrate a preference for binding with apo-CaM.[87,90]

In summary, the conformational dynamics of CaM and its complexes ($n$$Ca^{2+}$–CaM and $n$$Ca^{2+}$–CaM–Mel) were explored using an MCE and native MS based method. Although coarse grained structure information was acquired, MCE–native MS is a relatively rapid technique for characterizing protein conformations under various conditions without the need for crystallization and chemical labeling. Key observations are as follows: 1. CaM molecules, whether bound to Ca^{2+} or not, actively "jump" (equilibrium exchange) between open and closed conformations in liquid environments. 2. In the closed conformation, CaM and Ca^{2+}-bound CaM behave as globular proteins that have a single charge distribution in the native mass spectrum. In the closed conformation, CaM prefers to add $2Ca^{2+}$ and $4Ca^{2+}$ depending on the concentration of Ca^{2+}. 3. In the open conformation, CaM and Ca^{2+}-bound CaM have multimodal distributions in their native mass spectra, indicating the presence of IDRs. No preference was observed in terms of the number of Ca^{2+} added to CaM. 4. No discernible conformational change was observed following the binding of various Ca^{2+} (from 1 to 4). The portion of IDRs was not decreased after the binding of Ca^{2+}. 5. Besides the $4Ca^{2+}$–CaM–Mel complex, the $3Ca^{2+}$–CaM–Mel complex was also observed at a relatively low Ca^{2+} concentration. 6. The coexistence of diverse conformations allows for the recognition of multiple targets, while binding to varying numbers of Ca^{2+} could provide different amounts of hydrophobic pockets, further promoting complex formation. This MCE–native MS based method has revealed the relationship between the conformation of CaM and the number of Ca^{2+} bound, and it has unveiled the possible mechanisms of interaction between CaM and ligands. This coarse grained approach can compensate for the limitations of X-ray, NMR and other techniques in explaining protein dynamics, becoming an important supplementary method for studying protein structure and function.

Materials and methods

Chemicals

Commercial recombinant bovine CaM (Sigma Aldrich, St Louis, MO, USA) was dissolved in 20 mM ammonium acetate at a concentration of 20 μM. The chelating agent, EDTA (25 mM), was then added to dissociate CaM–metal ion complexes, and ultrafiltration was performed to remove Ca^{2+} residues. $CaCl_2$ was then added with concentration varying from 0 to 80 μM. Calcium chloride ($CaCl_2$) and ethylenediaminetetraacetic acid (EDTA) were purchased from Thermo Fisher Scientific (Massachusetts, USA). Formic acid and ammonia solution (Dikma, Beijing, China) were used to adjust pH. Melittin (Mel) was purchased from APExBIO (Houston, USA). Ammonia solution (25%) was purchased from Fuchen (Tianji, China). Phenol was obtained from Innochem (Beijing, China). The coated capillary was purchased from Sino Sumtech (Hebei, China). A water bath was used to control the reaction temperature of CaM and $CaCl_2$. All mixtures were incubated at room temperature for 30 minutes, except for the temperature-controlled experiments, in which samples were pre-incubated at different temperatures for 30 minutes right before the ESI analyses.

MCE experiments

MCE experiments were performed on an Agilent 7100 CE system (Agilent technology, USA). The coated capillary used in the MCE experiment has an inner diameter of 75 μm, a total length of 48.5 cm and an effective length of 40 cm. Phenol was added to a final concentration of 1/6000 (v/v) for each sample as the neutral marker. Before each sample injection, the capillary should be rinsed with 20 mM H_3PO_4 for 3 min and then with 20 mM ammonium acetate (pH 7.0) buffer for 3 min. Samples were injected at a pressure of 50 mbar for 5 s and separated by applying a 10 kV/15 kV DC separation voltage for $n$$Ca^{2+}$–CaM and $n$$Ca^{2+}$–CaM–Mel, respectively, and a 30 mbar driving pressure simultaneously. The samples were detected at a wavelength of 214 nm. The working temperature of the capillary was set at 25 °C in all experiments.

Native MS experiments

Native mass spectra were acquired using an Xevo G2-XS TOF, where 10 μL samples were loaded in the nano electrospray ionization (nESI) glass capillary for analysis. All samples were analyzed under the positive ion mode. The MS parameters used in this work were as follows: spray voltage: 2.8 kV; sampling cone voltage: 60 V; source temperature: 150 °C; desolvation temperature: 400 °C; cone gas flow: 50 L h^{-1}; desolvation flow: 600 L h^{-1}; acquisition rate: 1 spectra per s; MS scan range: 400–5000 Th.

Str2str. Given 1PRW as the initial structure, the backbone frames were sampled through the forward–backward process. The output was a set of global coordinates for the backbone atoms. The side chain conformations were predicted using the backbone-dependent rotamer libraries. The process minimized energy through a Monte Carlo searching scheme, ensuring that the sampled conformations were physically plausible. Open-source implementation is available at **https://github.com/lujiarui/Str2Str**.

Author contributions

Yi Zhao: data curation, formal analysis, investigation, methodology and writing. Wenjing Zhang: formal analysis and methodology. Jie Hong: data curation. Lei Yang: data curation. Yuanyuan Wang: conceptualization. Feng Qu: project administration. Wei Xu: conceptualization, funding acquisition, methodology, project administration, resources, software, supervision and writing.

Conflicts of interest

There are no conflicts to declare.

Acknowledgements

This work was supported by NNSFC (22374009). We also thank the Analysis & Testing Center of the Beijing Institute of Technology for MS instrument support.

References

1 D. Vinayagam, D. Quentin, J. Yu-Strzelczyk, O. Sitsel, F. Merino, M. Stabrin, O. Hofnagel, M. Yu, M. W. Ledeboer, G. Nagel, G. Malojcic and S. Raunser, Structural basis of TRPC4 regulation by calmodulin and pharmacological agents, *eLife*, 2020, **9**, e60603.

2 W. Tian, C. Hou, Z. Ren, C. Wang, F. Zhao, D. Dahlbeck, S. Hu, L. Zhang, Q. Niu, L. Li, B. J. Staskawicz and S. Luan, A calmodulin-gated calcium channel links pathogen patterns to plant immunity, *Nature*, 2019, **572**(7767), 131–135.

3 C. H. Lee and R. MacKinnon, Activation mechanism of a human SK-calmodulin channel complex elucidated by cryo-EM structures, *Science*, 2018, **360**(6388), 508–513.

4 C. Léger, I. Pitard, M. Sadi, N. Carvalho, S. Brier, A. Mechaly, D. Raoux-Barbot, M. Davi, S. Hoos, P. Weber, P. Vachette, D. Durand, A. Haouz, J. I. Guijarro, D. Ladant and A. Chenal, Dynamics and structural changes of calmodulin upon interaction with the antagonist calmidazolium, *BMC Biol.*, 2022, **20**(1), 176.

5 J. Wang, Q. Zhang, Y. Li, X. Pan, Y. Shan and J. Zhang, Remodeling the tumor microenvironment by vascular normalization and GSH-depletion for augmenting tumor immunotherapy, *Chin. Chem. Lett.*, 2024, **35**(2), 108746.

6 J. Wang, X. Pan, J. Zhang, Q. Zhang, Y. Li, W. Guo and J. Zhang, Active molecule-based theranostic agents for tumor vasculature normalization and antitumor efficacy, *Chin. Chem. Lett.*, 2023, 109187.

7 Y. S. Babu, J. S. Sack, T. J. Greenhough, C. E. Bugg, A. R. Means and W. J. Cook, Three-dimensional structure of calmodulin, *Nature*, 1985, **315**(6014), 37–40.

8 H. Kuboniwa, N. Tjandra, S. Grzesiek, H. Ren, C. B. Klee and A. Bax, Solution structure of calcium-free calmodulin, *Nat. Struct. Biol.*, 1995, **2**(9), 768–776.

9 M. A. Schumacher, A. F. Rivard, H. P. Bächinger and J. P. Adelman, Structure of the gating domain of a Ca^{2+}-activated K^{+} channel complexed with Ca^{2+}/calmodulin, *Nature*, 2001, **410**(6832), 1120–1124.

10 D. Shukla, A. Peck and V. S. Pande, Conformational heterogeneity of the calmodulin binding interface, *Nat. Commun.*, 2016, **7**, 10910.

11 M. Zhang, T. Tanaka and M. Ikura, Calcium-induced conformational transition revealed by the solution structure of apo calmodulin, *Nat. Struct. Biol.*, 1995, **2**(9), 758–767.

12 R. Chattopadhyaya, W. E. Meador, A. R. Means and F. A. Quiocho, Calmodulin structure refined at 1.7 A resolution, *J. Mol. Biol.*, 1992, **228**(4), 1177–1192.

13 S. T. Rao, S. Wu, K. A. Satyshur, K. Y. Ling, C. Kung and M. Sundaralingam, Structure of Paramecium tetraurelia calmodulin at 1.8 A resolution, *Protein Sci.*, 1993, **2**(3), 436–447.

14 M. A. Wilson and A. T. Brunger, The 1.0 A crystal structure of Ca(2+)-bound calmodulin: an analysis of disorder and implications for functionally relevant plasticity, *J. Mol. Biol.*, 2000, **301**(5), 1237–1256.

15 C. Ban, B. Ramakrishnan, K. Y. Ling, C. Kung and M. Sundaralingam, Structure of the recombinant Paramecium tetraurelia calmodulin at 1.68 A resolution, *Acta Crystallogr., Sect. D: Biol. Crystallogr.*, 1994, **50**(Pt 1), 50–63.

16 C. H. Yun, J. Bai, D. Y. Sun, D. F. Cui, W. R. Chang and D. C. Liang, Structure of potato calmodulin PCM6: the first report of the three-dimensional structure of a plant calmodulin, *Acta Crystallogr., Sect. D: Biol. Crystallogr.*, 2004, **60**(Pt 7), 1214–1219.

17 M. K. Joshi, S. Moran, K. M. Beckingham and K. R. MacKenzie, Structure of androcam supports specialized interactions with myosin VI, *Proc. Natl. Acad. Sci. U. S. A.*, 2012, **109**(33), 13290–13295.

18 M. Osawa, M. B. Swindells, J. Tanikawa, T. Tanaka, T. Mase, T. Furuya and M. Ikura, Solution structure of calmodulin-W-7 complex: the basis of diversity in molecular recognition, *J. Mol. Biol.*, 1998, **276**(1), 165–176.

19 W. E. Meador, A. R. Means and F. A. Quiocho, Target enzyme recognition by calmodulin: 2.4 A structure of a calmodulin-peptide complex, *Science*, 1992, **257**(5074), 1251–1255.

20 H. Kurokawa, M. Osawa, H. Kurihara, N. Katayama, H. Tokumitsu, M. B. Swindells, M. Kainosho and M. Ikura, Target-induced conformational adaptation of calmodulin revealed by the crystal structure of a complex with nematode Ca(2+)/calmodulin-dependent kinase peptide, *J. Mol. Biol.*, 2001, **312**(1), 59–68.

21 K. L. Yap, T. Yuan, T. K. Mal, H. J. Vogel and M. Ikura, Structural basis for simultaneous binding of two carboxy-terminal peptides of plant glutamate decarboxylase to calmodulin, *J. Mol. Biol.*, 2003, **328**(1), 193–204.

22 V. Harmat, Z. Böcskei, G. Náray-Szabó, I. Bata, A. S. Csutor, I. Hermecz, P. Arányi, B. Szabó, K. Liliom, B. G. Vértessy and J. Ovádi, A new potent calmodulin antagonist with arylalkylamine structure: crystallographic, spectroscopic and functional studies, *J. Mol. Biol.*, 2000, **297**(3), 747–755.

23 S. Mirzoeva, S. Weigand, T. J. Lukas, L. Shuvalova, W. F. Anderson and D. M. Watterson, Analysis of the functional coupling between calmodulin's calcium binding and peptide recognition properties, *Biochemistry*, 1999, **38**(13), 3936–3947.

24 E. A. Hodge, M. A. Benhaim and K. K. Lee, Bridging protein structure, dynamics, and function using hydrogen/deuterium-exchange mass spectrometry, *Protein Sci.*, 2020, **29**(4), 843–855.

25 K. Henzler-Wildman and D. Kern, Dynamic personalities of proteins, *Nature*, 2007, **450**(7172), 964–972.

26 N. Will, K. Lee, F. Hajredini, D. H. Giles, R. R. Abzalimov, M. Clarkson, K. N. Dalby and R. Ghose, Structural Dynamics of the Activation of Elongation Factor 2 Kinase by Ca(2+)-Calmodulin, *J. Mol. Biol.*, 2018, **430**(17), 2802–2821.

27 T. S. Beyett, A. E. Fraley, E. Labudde, D. Patra, R. C. Coleman, A. Eguchi, A. Glukhova, Q. Chen, R. M. Williams, W. J. Koch, D. H. Sherman and J. J. G. Tesmer, Perturbation of the interactions of calmodulin with GRK5 using a natural product chemical probe, *Proc. Natl. Acad. Sci. U. S. A.*, 2019, **116**(32), 15895–15900.

28 T. Schmidt, J. Jeon, W. M. Yau, C. D. Schwieters, R. Tycko and G. M. Clore, Time-resolved DEER EPR and solid-state NMR afford kinetic and structural elucidation of substrate binding to Ca(2+)-ligated calmodulin, *Proc. Natl. Acad. Sci. U. S. A.*, 2022, **119**(6), e2122308119.

29 N. Karschin, S. Becker and C. Griesinger, Interdomain Dynamics via Paramagnetic NMR on the Highly Flexible Complex Calmodulin/Munc13–1, *J. Am. Chem. Soc.*, 2022, **144**(37), 17041–17053.

30 A. Piserchio, K. Long, K. Lee, E. A. Kumar, R. Abzalimov, K. N. Dalby and R. Ghose, Structural dynamics of the complex of calmodulin with a minimal functional construct of eukaryotic elongation factor 2 kinase and the role of Thr348 autophosphorylation, *Protein Sci.*, 2021, **30**(6), 1221–1234.

31 E. Nuñez, F. Jones, A. Muguruza-Montero, J. Urrutia, A. Aguado, C. Malo, G. Bernardo-Seisdedos, C. Domene, O. Millet, N. Gamper and A. Villarroel, Redox regulation of K(v)7 channels through EF3 hand of calmodulin, *eLife*, 2023, **12**, 81961.

32 B. Sharma, S. K. Deo, L. G. Bachas and S. Daunert, Competitive binding assay using fluorescence resonance energy transfer for the identification of calmodulin antagonists, *Bioconjugate Chem.*, 2005, **16**(5), 1257–1263.

33 B. Zhang, Z. Gong, L. Zhao, Y. An, H. Gao, J. Chen, Z. Liang, M. Liu, Y. Zhang, Q. Zhao and L. Zhang, Decoding Protein Dynamics in Cells Using Chemical Cross-Linking and Hierarchical Analysis, *Angew. Chem., Int. Ed.*, 2023, **62**(35), e202301345.

34 Y. H. Ding, Z. Gong, X. Dong, K. Liu, Z. Liu, C. Liu, S. M. He, M. Q. Dong and C. Tang, Modeling Protein Excited-state Structures from "Over-length" Chemical Cross-links, *J. Biol. Chem.*, 2017, **292**(4), 1187–1196.

35 R. J. Yu, Y. L. Ying, Y. X. Hu, R. Gao and Y. T. Long, Label-Free Monitoring of Single Molecule Immunoreaction with a Nanopipette, *Anal. Chem.*, 2017, **89**(16), 8203–8206.

36 Q. Li, Y. L. Ying, S. C. Liu, Y. Lin and Y. T. Long, Detection of Single Proteins with a General Nanopore Sensor, *ACS Sens.*, 2019, **4**(5), 1185–1189.

37 S. S. Çınaroğlu and P. C. Biggin, The role of loop dynamics in the prediction of ligand-protein binding enthalpy, *Chem. Sci.*, 2023, **14**(24), 6792–6805.

38 K. Xue, K. T. Movellan, X. C. Zhang, E. E. Najbauer, M. C. Forster, S. Becker and L. B. Andreas, Towards a native environment: structure and function of membrane proteins in lipid bilayers by NMR, *Chem. Sci.*, 2021, **12**(43), 14332–14342.

39 G. Hu, H. Jia, L. Zhao, D.-H. Cho and J. Fang, Small molecule fluorescent probes of protein vicinal dithiols, *Chin. Chem. Lett.*, 2019, **30**(10), 1704–1716.

40 I. D. G. Campuzano, J. H. Robinson, J. O. Hui, S. D. Shi, C. Netirojjanakul, M. Nshanian, P. F. Egea, J. L. Lippens, D. Bagal, J. A. Loo and M. Bern, Native and Denaturing MS Protein Deconvolution for Biopharma: Monoclonal Antibodies and Antibody-Drug Conjugates to Polydisperse Membrane Proteins and Beyond, *Anal. Chem.*, 2019, **91**(15), 9472–9480.

41 H. Chen, L. S. Eberlin and R. G. Cooks, Neutral fragment mass spectra via ambient thermal dissociation of peptide and protein ions, *J. Am. Chem. Soc.*, 2007, **129**(18), 5880–5886.

42 B. Domon and R. Aebersold, Mass spectrometry and protein analysis, *Science*, 2006, **312**(5771), 212–217.

43 G. Li, A. Phetsanthad, M. Ma, Q. Yu, A. Nair, Z. Zheng, F. Ma, K. DeLaney, S. Hong and L. Li, Native Ion Mobility-Mass Spectrometry-Enabled Fast Structural Interrogation of Labile Protein Surface Modifications at the Intact Protein Level, *Anal. Chem.*, 2022, **94**(4), 2142–2153.

44 M. T. Marty, K. K. Hoi, J. Gault and C. V. Robinson, Probing the Lipid Annular Belt by Gas-Phase Dissociation

of Membrane Proteins in Nanodiscs, *Angew. Chem., Int. Ed.*, 2016, **55**(2), 550–554.

45 Z. Ouyang, Z. Takáts, T. A. Blake, B. Gologan, A. J. Guymon, J. M. Wiseman, J. C. Oliver, V. J. Davisson and R. G. Cooks, Preparing protein microarrays by soft-landing of mass-selected ions, *Science*, 2003, **301**(5638), 1351–1354.

46 A. Phetsanthad, G. Li, C. K. Jeon, B. T. Ruotolo and L. Li, Comparing Selected-Ion Collision Induced Unfolding with All Ion Unfolding Methods for Comprehensive Protein Conformational Characterization, *J. Am. Soc. Mass Spectrom.*, 2022, **33**(6), 944–951.

47 C. Schmidt, M. Zhou, H. Marriott, N. Morgner, A. Politis and C. V. Robinson, Comparative cross-linking and mass spectrometry of an intact F-type ATPase suggest a role for phosphorylation, *Nat. Commun.*, 2013, **4**, 1985.

48 M. Valletta, S. Ragucci, N. Landi, A. Di Maro, P. V. Pedone, R. Russo and A. Chambery, Mass spectrometry-based protein and peptide profiling for food frauds, traceability and authenticity assessment, *Food Chem.*, 2021, **365**, 130456.

49 Z. Wei, Z. Xie, R. Kuvelkar, V. Shah, K. Bateman, D. G. McLaren and R. G. Cooks, High-Throughput Bioassays using "Dip-and-Go" Multiplexed Electrospray Mass Spectrometry, *Angew. Chem., Int. Ed.*, 2019, **58**(49), 17594–17598.

50 H. Wu, R. Zhang, W. Zhang, J. Hong, Y. Xiang and W. Xu, Rapid 3-dimensional shape determination of globular proteins by mobility capillary electrophoresis and native mass spectrometry, *Chem. Sci.*, 2020, **11**(18), 4758–4765.

51 W. Zhang, H. Wu, R. Zhang, X. Fang and W. Xu, Structure and effective charge characterization of proteins by a mobility capillary electrophoresis based method, *Chem. Sci.*, 2019, **10**(33), 7779–7787.

52 L. Yang, W. Zhang and W. Xu, Efficient protein conformation dynamics characterization enabled by mobility-mass spectrometry, *Anal. Chim. Acta*, 2023, **1243**, 340800.

53 W. Zhang, J. Hong, L. Yang, Z. Xu, Y. Xiang and W. Xu, Resolving the geometric structure of trastuzumab by mobility capillary electrophoresis and native mass spectrometry, *Chin. Chem. Lett.*, 2023, 108695.

54 W. Zhang, Y. Xiang and W. Xu, Probing protein higher-order structures by native capillary electrophoresis-mass spectrometry, *TrAC, Trends Anal. Chem.*, 2022, **157**, 116739.

55 I. A. Kaltashov and A. Mohimen, Estimates of protein surface areas in solution by electrospray ionization mass spectrometry, *Anal. Chem.*, 2005, **77**(16), 5370–5379.

56 L. Testa, S. Brocca and R. Grandori, Charge-surface correlation in electrospray ionization of folded and unfolded proteins, *Anal. Chem.*, 2011, **83**(17), 6459–6463.

57 K. Chingin and K. Barylyuk, Charge-State-Dependent Variation of Signal Intensity Ratio between Unbound Protein and Protein-Ligand Complex in Electrospray Ionization Mass Spectrometry: The Role of Solvent-Accessible Surface Area, *Anal. Chem.*, 2018, **90**(9), 5521–5528.

58 D. Stuchfield and P. Barran, Unique insights to intrinsically disordered proteins provided by ion mobility mass spectrometry, *Curr. Opin. Chem. Biol.*, 2018, **42**, 177–185.

59 R. Beveridge, L. G. Migas, R. K. Das, R. V. Pappu, R. W. Kriwacki and P. E. Barran, Ion Mobility Mass Spectrometry Uncovers the Impact of the Patterning of Oppositely Charged Residues on the Conformational Distributions of Intrinsically Disordered Proteins, *J. Am. Chem. Soc.*, 2019, **141**(12), 4908–4918.

60 N. Khristenko, F. Rosu, E. Largy, J. Haustant, C. Mesmin and V. Gabelica, Native Electrospray Ionization of Multi-Domain Proteins via a Bead Ejection Mechanism, *J. Am. Chem. Soc.*, 2023, **145**(1), 498–506.

61 J. L. Fallon and F. A. Quiocho, A closed compact structure of native Ca(2+)-calmodulin, *Structure*, 2003, **11**(10), 1303–1307.

62 B. D. Slaughter, J. R. Unruh, E. S. Price, J. L. Huynh, R. J. Bieber Urbauer and C. K. Johnson, Sampling unfolding intermediates in calmodulin by single-molecule spectroscopy, *J. Am. Chem. Soc.*, 2005, **127**(34), 12107–12114.

63 C. K. Johnson, Calmodulin, conformational states, and calcium signaling. A single-molecule perspective, *Biochemistry*, 2006, **45**(48), 14233–14246.

64 T. Schmidt, D. Wang, J. Jeon, C. D. Schwieters and G. M. Clore, Quantitative agreement between conformational substates of holo calcium-loaded calmodulin detected by double electron–electron resonance EPR and predicted by molecular dynamics simulations, *J. Am. Chem. Soc.*, 2022, **144**(27), 12043–12051.

65 M. Luan, Z. Hou, B. Zhang, L. Ma, S. Yuan, Y. Liu and G. Huang, Inter-Domain Repulsion of Dumbbell-Shaped Calmodulin during Electrospray Ionization Revealed by Molecular Dynamics Simulations, *Anal. Chem.*, 2023, **95**(23), 8798–8806.

66 J. Jeon, W. M. Yau and R. Tycko, Millisecond Time-Resolved Solid-State NMR Reveals a Two-Stage Molecular Mechanism for Formation of Complexes between Calmodulin and a Target Peptide from Myosin Light Chain Kinase, *J. Am. Chem. Soc.*, 2020, **142**(50), 21220–21232.

67 W. P. Hall, J. N. Anker, Y. Lin, J. Modica, M. Mrksich and R. P. Van Duyne, A calcium-modulated plasmonic switch, *J. Am. Chem. Soc.*, 2008, **130**(18), 5836–5837.

68 H. Y. Park, S. A. Kim, J. Korlach, E. Rhoades, L. W. Kwok, W. R. Zipfel, M. N. Waxham, W. W. Webb and L. Pollack, Conformational changes of calmodulin upon Ca^{2+} binding studied with a microfluidic mixer, *Proc. Natl. Acad. Sci. U. S. A.*, 2008, **105**(2), 542–547.

69 V. Muñoz, Conformational dynamics and ensembles in protein folding, *Annu. Rev. Biophys. Biomol. Struct.*, 2007, **36**, 395–412.

70 J. Lu, B. Zhong, Z. Zhang and J. Tang, in *Str2str: A score-based framework for zero-shot protein conformation sampling*, The Twelfth International Conference on Learning Representations, 2023.

71 Y. Yamada, T. Matsuo, H. Iwamoto and N. Yagi, A compact intermediate state of calmodulin in the process of target binding, *Biochemistry*, 2012, **51**(19), 3963–3970.

72 J. F. Zhang, L. Ma, X. Liu and Y. T. Lu, Using capillary electrophoresis with laser-induced fluorescence to study the interaction of green fluorescent protein-labeled calmodulin with Ca^{2+}- and calmodulin-binding protein, *J. Chromatogr. B: Anal. Technol. Biomed. Life Sci.*, 2004, **804**(2), 413–420.

73 A. Levin and T. J. Blanck, Halothane and isoflurane alter the Ca^{2+} binding properties of calmodulin, *Anesthesiology*, 1995, **83**(1), 120–126.

74 O. Nemirovskiy, D. E. Giblin and M. L. Gross, Electrospray ionization mass spectrometry and hydrogen/deuterium exchange for probing the interaction of calmodulin with calcium, *J. Am. Soc. Mass Spectrom.*, 1999, **10**(8), 711–718.

75 S. Pepke, T. Kinzer-Ursem, S. Mihalas and M. B. Kennedy, A dynamic model of interactions of Ca^{2+}, calmodulin, and catalytic subunits of Ca^{2+}/calmodulin-dependent protein kinase II, *PLoS Comput. Biol.*, 2010, **6**(2), e1000675.

76 J. S. Smith, E. Rousseau and G. Meissner, Calmodulin modulation of single sarcoplasmic reticulum Ca^{2+}-release channels from cardiac and skeletal muscle, *Circ. Res.*, 1989, **64**(2), 352–359.

77 M. Marcinkowski, T. Pilžys, D. Garbicz, J. Piwowarski, K. Przygońska, M. Winiewska-Szajewska, K. Ferenc, O. Skorobogatov, J. Poznański and E. Grzesiuk, Calmodulin as Ca(2+)-Dependent Interactor of FTO Dioxygenase, *Int. J. Mol. Sci.*, 2021, **22**(19), 10869.

78 J. Y. Chang, Y. Nakahata, Y. Hayano and R. Yasuda, Mechanisms of Ca(2+)/calmodulin-dependent kinase II activation in single dendritic spines, *Nat. Commun.*, 2019, **10**(1), 2784.

79 Z. Dürvanger, T. Juhász, K. Liliom and V. Harmat, Structures of calmodulin-melittin complexes show multiple binding modes lacking classical anchoring interactions, *J. Biol. Chem.*, 2023, **299**(4), 104596.

80 P. Csermely, R. Palotai and R. Nussinov, Induced fit, conformational selection and independent dynamic segments: an extended view of binding events, *Trends Biochem. Sci.*, 2010, **35**(10), 539–546.

81 L.-P. Yang, L. Zhang, M. Quan, J. S. Ward, Y.-L. Ma, H. Zhou, K. Rissanen and W. Jiang, A supramolecular system that strictly follows the binding mechanism of conformational selection, *Nat. Commun.*, 2020, **11**(1), 2740.

82 E. Yamauchi, T. Nakatsu, M. Matsubara, H. Kato and H. Taniguchi, Crystal structure of a MARCKS peptide containing the calmodulin-binding domain in complex with Ca^{2+}-calmodulin, *Nat. Struct. Mol. Biol.*, 2003, **10**(3), 226–231.

83 V. Schauer-Vukasinovic, L. Cullen and S. Daunert, Rational design of a calcium sensing system based on induced conformational changes of calmodulin, *J. Am. Chem. Soc.*, 1997, **119**(45), 11102–11103.

84 A. I. Denesyuk, S. E. Permyakov, E. A. Permyakov, M. S. Johnson, K. Denessiouk and V. N. Uversky, Canonical structural-binding modes in the calmodulin–target protein complexes, *J. Biomol. Struct. Dyn.*, 2023, **41**(16), 7582–7594.

85 W. E. Meador, A. R. Means and F. A. Quiocho, Target enzyme recognition by calmodulin: 2.4 Å structure of a calmodulin-peptide complex, *Science*, 1992, **257**(5074), 1251–1255.

86 B. Chagot and W. J. Chazin, Solution NMR structure of Apo-calmodulin in complex with the IQ motif of human cardiac sodium channel NaV1.5, *J. Mol. Biol.*, 2011, **406**(1), 106–119.

87 J. B. Yoder, M. Ben-Johny, F. Farinelli, L. Srinivasan, S. R. Shoemaker, G. F. Tomaselli, S. B. Gabelli and L. M. Amzel, Ca(2+)-dependent regulation of sodium channels Na(v)1.4 and Na(v)1.5 is controlled by the post-IQ motif, *Nat. Commun.*, 2019, **10**(1), 1514.

88 S. Kumar, S. Aslam, M. Mazumder, P. Dahiya, A. Murmu, B. A. Manjasetty, R. Zaidi, A. Bhattacharya and S. Gourinath, Crystal structure of calcium binding protein-5 from Entamoeba histolytica and its involvement in initiation of phagocytosis of human erythrocytes, *PLoS Pathog.*, 2014, **10**(12), e1004532.

89 H. Wang, X. Liu, J. Zhao, Q. Yue, Y. Yan, Z. Gao, Y. Dong, Z. Zhang, Y. Fan, J. Tian, N. Wu and Y. Gong, Crystal structures of multicopper oxidase CueO G304K mutant: structural basis of the increased laccase activity, *Sci. Rep.*, 2018, **8**(1), 14252.

90 M. D. Feldkamp, L. Yu and M. A. Shea, Structural and energetic determinants of apo calmodulin binding to the IQ motif of the NaV1. 2 voltage-dependent sodium channel, *Structure*, 2011, **19**(5), 733–747.